Two-Dimensional Analysis of Flow Field and Associated Scour Parameters at Downstream of Weir with and without Sloping Apron

R. Karthik[1], U. Kumar[2], and A.K. Barbhuiya[3]

[1]Research Scholar, Civil Engineering Department, NIT Silchar

[2]Associate Professor, Civil Engineering Department, NIT Silchar

[3]Professor, Civil Engineering Department, NIT Silchar

Corresponding author: R. Karthik, Email: civilkarthik2010@gmail.com

Abstract

The downstream scour of the control structure is more common and very complex issue in the river engineering now-a-days. Flow-features in the vicinity of control structure are quite different from other parts of the river. In order to visualise the flow features precisely in the vicinity of the control structure, the combination of Multiphase Eulerian model (Ansys 17 Fluent) and hybrid Dense Discrete Phase Model (DDPM) is primarily employed in the present research work. These models provide better visualisation of the flow structure and its associated scour development both in the upstream as well as in the downstream direction. Here initially, the model simulation is performed with trapezoidal weir and trapezoidal weir with sloping apron platforms and then comparison is made between the flow -structure and their associated scour. The erosion is computed by Mc Laury erosion model and particle tracking is done using DDPM through a Lagrangian approach which helps in stimulating the movement of the particles within flow domain, as well as the velocity and other properties. Besides this, sediment particle tracking is also shown in the above-mentioned research work. The obtained results show that the velocity of the flow reaches around 0.835 ms $^{-1}$ using trapezoidal weir. However, as in case of trapezoidal weir with sloping apron, the maximum velocity goes approximately 0.505 ms^{-1} which is almost equal to inlet velocity. Hence, sloping apron plays a significant role in protecting the downstream side of control structure.

Key words: CFD, Mc Laury erosion model, K- ε Turbulence model, DDPM, Eulerian approach, Fluent

1 Introduction

From past years, river restoration has been emerged as a significant topic to improve Rivers Bathymetry. Rivers are highly turbulence, meander and braided in nature. The carrying capacity of the channel is influenced by cross sectional shape of the channel for braided rivers; the carrying capacity is reduced due to formation of shoals which leads to flooding. To avoid this situation different river restoration practice being practiced, constructing grade control structure across the entire width of the river is one of such measures. Grade control structure like weir not only limited to maintain the cross sectional shape of the channel but also provides head water storage along with protecting bank from erosion. The effect of jet overflow at downstream structure leads towards development of scour hole. Due to development of scour hole which undermine the foundation of the structure and leads to its failure. (Bormann, N. E., and Julien, P. Y. 1991).

Since from 1932, numerous research works have been carried out on the flow structure and scour hole formation at downstream of grade control structures. Rajaratnam, N., and Nwachukwu, B. A. (1983) and Bormann, N. E., and Julien, P. Y. (1991), D'Agostino, V., and Ferro, V (2004), Dey, S., and Sarkar, A. (2006), Pagliara, S., e al. (2015) and many more studied the flow and scour parameters experimentally and found expression to predict the scour profile like maximum length, depth of the scour hole and impacting features of scour formation like tail water depth, height of the structure and ratio of upstream and downstream water depth etc. Kang, S., & Sotiropoulos, F. (2015) has studied the flow dynamics near

the control structure numerically, Muller, S. et al. (2011) has studied the bed particle deformation in front of weir.

Measures for protection against erosion are very costly as it requires, protection of huge area of the bed. Moreover it is experienced that some shear failure at end of the bed protection and subsequent progressive scour process leads to the failure of the structure (G.J.C.M. Hoffmans and K.W. Pilarczyk 1995). To overcome these issues and to design an efficient control structure, designers need to have deep knowledge of the downstream flow structure and associated scour parameters. However some features of the flow and scour mechanisms either could not be visualized in the laboratory or field study, are very costly and time consuming. Therefore Computational Fluid Dynamics (CFD) is the tool which can easily be used to identify or to visualize these characteristics. In the recent years wide range of hydraulic parameters studied with CFD become much cost effective as reported by Lv, X., Zou, Q., and Reeve, D. (2011) in the recent years. Development of Computing power and sophisticated CFD codes in the recent years are playing a vital role in the hydraulic and river engineering research (Nguyen, V. T., and Nestmann, F. (2004). Many researchers like Tingsanchali, T., and Maheswaran, S. (1990), Sinha, S. K., and Marelius, F. (2000), Weidner et al. (2012), Mario Oertel et al. (2015), Nguyen, V. T., Moreno, C. S., and Lyu, S. (2015) and others studied the flow and scour profile at downstream of grade control structure. Nowadays many commercial and open sources CFD software's are available, among Ansys Fluent Software is such one which is widely used to solve industrial oriented problem because it offers wide variety of simulation option with different numerical algorithms. K-ε turbulence model together with VOF model is well capable to simulate the flow field over weir in rectangular channel (Qu, J., Ramamurthy, A. S., Tadayon, R., and Chen, Z. (2009). Mazdak Parsi et al. (2016) had studied Sand particle erosion with multiphase flow condition by using super computer having 256 cores computational power with Ansys fluent VOF model for run-time of 30 sec. Mc Laury erosion model is widely used in oil and gas field to study the erosion behavior of slurry flows at the surface of pipe but has not been utilized by any other researchers to study the erosion behavior in river engineering.

The main objective of this article is to identify the cause and effects of scour hole in upstream and downstream of the trapezoidal weir and trapezoidal weir with sloping apron. This results in reviews various flow structure and sediment properties. Most of the studies concentrated only on experimentally to study flow structure and downstream scour. Based on our knowledge there is no such article focused on computationally study the flow, scour at downstream and particle tracking by Ansys Fluent in river engineering.

2. Model Description

The simulation of flow features and other parameters in 3D is very costly because its require high computing power and time consuming though, the flow features is not varying much with respect of width of the channel, so the present study carried out with 2D case. The 2D model of flow domain with sand bed was created using Ansys Design modeler, which displayed in Fig.1, total length of the flow domain was 8 m and depth of the flow domain was 1 m including 20 cm sand bed and 80 cm flow depth. The trapezoidal weir was located at 3 m from inlet having base width 30 cm, top width 10 cm and height 40 cm was considered. Downstream sloping apron is having 70 cm length, 30 cm depth with 10 cm end sill and sloping bucket radius was 18 cm is considered in the present model. The simulation of flow and erosion with trapezoidal weir is designated as 'case A' and simulation of flow and erosion with trapezoidal weir with sloping apron is designated as 'case B' for ease of understanding. In case A the trapezoidal structure starts and ends at 3m and 3.3m from inlet respectively. In case B the trapezoidal structure with sloping apron starts and ends at 3m and 4m form inlet respectively with the length of

sloping apron being 0.7m. This study was mainly consent about to study the flow features at vicinity of the control structure, so at the weir location from the inlet the flow may developed well and downstream of the structure had a sufficient length to visualize the flow features.

Meshing is the process to discretize the entire domain into number of smaller, non-overlapping sub-elements. Quality of solution and Stability of solution (convergence/divergence) was strongly depending on the mesh quality. In the present study meshing was done by Ansys meshing. Three different Quality of mesh like coarse, medium and fine were carried out to ensure that the result is mesh independent (Mevlut Sami Akoz et al. 2014). Number of elements in the normal weir model was 338,244 and weir with sloping apron was 283,643. Five numbers of inflation layers was given all the boundary surfaces to well capture the property near wall surfaces. Mesh Quality like element quality, Skewness and orthogonal quality have been checked and it have fulfilled the requirements as mentioned by M.M. Noor, (2013).

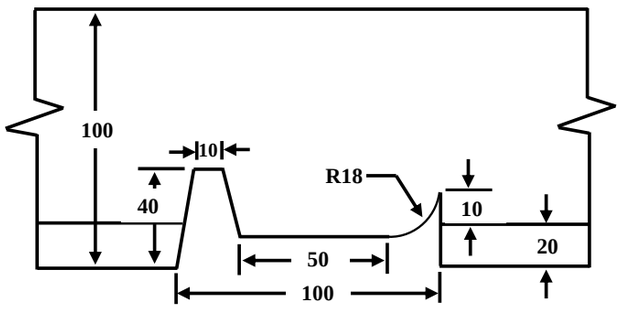

Trapezoidal weir with sloping apron

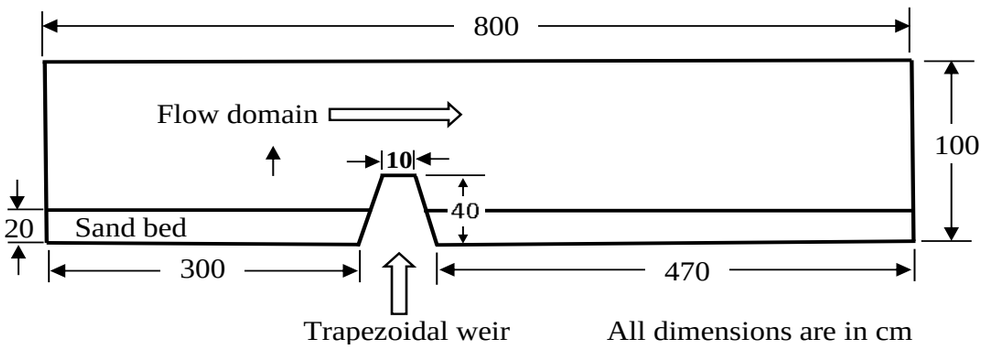

Figure 1. Flow domain and sand bed with trapezoidal weir with sloping apron at end

3. Numerical Model

Among other CFD software's Ansys Fluent 18.0 software is sophisticated and offers many simulation options for different flow condition. The flow domain and sand bed involved in the present study, as a multiphase condition. The fluent software can effectively simulate the multiphase condition with Eulerian method. The fluent software could effectively track sand particle by means of Discrete Phase Method (DPM) and Dense Discrete Phase Method (DDPM). The DPM can track only 10% particle load but DDPM can track more than 10% particle load from the total particles. This simulation with support of Ansys Fluent multiphase model Eulerian with DDPM which is a hybrid model combines the Eulerrian-Lagrangian approach; where the flow is simulated by Eulerian method and particle tracking is done by Lagrangian method. Ansys Fluent software has several erosion models among Mc Laury erosion

model can effectively simulate erosion behavior of the slurry flows. So Mc. Laury model was implied in the present study to predict the erosion rate at downstream of the structure.

3.1 Continuity Equation for DDPM

$$\frac{\partial}{\partial_t}\left(\alpha_p \rho_p\right) + \nabla.\left(\alpha_p \rho_p \vec{v}_p\right) = \sum_{q=1}^{nphases}\left(\dot{m}_{qp} - \dot{m}_{qp}\right)$$

Where, $\vec{v}_p$ is the velocity of phase p and $\dot{m}_{qp}$ is characterizes the mass transfer from the "q" phase to "p" phase and $\dot{m}_{qp}$ is characterizes the mass transfer from the "p" phase to "q" phase. α_p And ρ_p is the volume fraction and density of the phase p.

3.2 Momentum Equation for DDPM

$$\frac{\partial}{\partial_t}\left(\alpha_p \rho_p \vec{v}_p\right) + \nabla.\left(\alpha_p \rho_p \vec{v}_p \vec{v}_p\right) = -\alpha_p \nabla_p + \nabla.\left[\alpha_p \mu_p \left(\nabla \vec{v}_p + \nabla \overrightarrow{v_p^T}\right)\right]$$

$$+\alpha_p \rho_p \overrightarrow{g} + F_{vm,lift,user} + \sum_{q=1}^{nphases}\left(\vec{K}_{qp}\left(\vec{v}_q - \vec{v}_p\right) + \dot{m}_{qp}\vec{v}_{qp} - \dot{m}_{qp}\vec{v}_{qp}\right)$$

$$+K_{DPM}\left(\vec{v}_{DPM} - \vec{v}_p\right) + S_{DPM,explicit}$$

Where, μ_p is the shear viscosity of phase p, $F_{vm,lift,user}$ is virtual mass force, lift force and user specified force. $S_{DPM,explicit}$ and $\vec{v}_{DPM}$ are momentum exchange term for explicit and implicit. K_{DPM} is particle averaged interphase momentum exchange coefficient.

3.3 Realizable K-ε Turbulence model

$$\frac{\partial}{\partial_t}(pk) + \frac{\partial}{\partial_{xj}}\left(\rho k u_j\right) = \frac{\partial}{\partial_{xj}}\left[\left(\mu + \frac{\mu_t}{\sigma_k}\right)\frac{\partial_k}{\partial_{xj}}\right] + G_k + G_b - \rho\varepsilon - Y_m + S_k$$

And

$$\frac{\partial}{\partial_t}(\rho\varepsilon) + \frac{\partial}{\partial_{xj}}\left(\rho\varepsilon u_j\right) = \frac{\partial}{\partial_{xj}}\left[\left(\mu + \frac{\mu_t}{\sigma_\varepsilon}\right)\frac{\partial_\varepsilon}{\partial_{xj}}\right] + \rho C_1 S_\varepsilon - \rho C_2 \frac{\varepsilon^2}{k + \sqrt{v\varepsilon}} + C_{1\varepsilon}\frac{\varepsilon}{k}C_{3\varepsilon}G_b + S_\varepsilon$$

Where

$$C_1 = max\left[0.43, \frac{\eta}{\eta+5}\right] \quad \eta = S\frac{k}{\varepsilon} \;, \quad S = \sqrt{2S_{ij}S_{ij}}$$

G_k is generation of turbulence kinetic energy due to mean velocity gradients; G_b is generation of turbulence kinetic energy due to buoyancy. C_2, $C_{3\varepsilon}$ and $C_{1\varepsilon}$ are constants. σ_k and σ_ε are the turbulent Prandtl numbers for K and ε respectively. S_k and S_ε are User-defined source term. Y_m is representing the contribution of the fluctuating dilation in compressible turbulence to the overall dissipation rate, S is the modulus of the mean rate-of-strain tensor.

3.4 Mc Laury Erosion Model

$$E = AV^n f(\gamma)$$

$$A = F\,Bh^k$$

$$f(\gamma) = b\gamma^2 + c\gamma$$

Where F is empirical constant, V is particle impact velocity, Bh is brinell's hardness number of wall material, K is constant for material property and γ is the particle impingement angle and b, c are the constant.

4. Boundary Condition

This simulation was conducted by using Intel core i7 machine with 4 parallel processing. In zone condition, primary phase was selected as water and secondary phase was selected as sand. Inlet chosen as a velocity inlet with initial velocity is of 0.5 ms^{-1}, outlet was pressure outlet, and top portion of flow domain was exposed to atmospheric pressure. Sand particle is considered as inert particle and particle injection was selected as a surface injection, sand particle initial velocity was set as zero. Particle distribution is not linear, fluent offers Rosin-Rammler equation to fitting the particle size distribution with different mass fraction by putting minimum, maximum and mean size of the particles. Two-way turbulence coupling is enabled to consider the effect created by particle in the flow domain and vice-versa. The under relaxation factor URF from solution control was given as 0.3 and 0.7 for Momentum and pressure to ensure solution stabilization. A time step size was 0.01 sec, total number of time step was 5000 and per time step 20 numbers of iteration was given, totally one lakh numbers of iteration was given and it took nearly 72 hours to complete the simulation for the run time of 50 sec. The particle injection was started at 3 sec, because the flow was well developed and capable to carry those particles at this stage and every 0.01 sec of time step particles was released from the top surface of sand bed and finally particles injection was stopped at 5 sec due to the limitation of computing power.

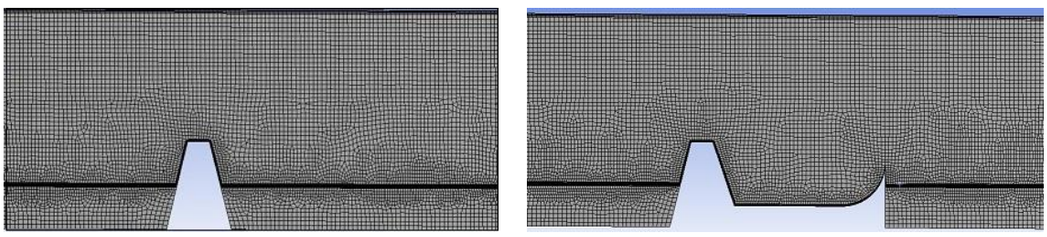

Figure 2. Closer view of mesh at Trapezoidal weir and Weir with Sloping apron.

Table 1 Sand Particle properties.

Density	1850 kg m^{-3}
Particle Distribution	Rosin-Rammler
Starting time of particle injection	3 sec
Finishing time of particle injection	5 sec
Minimum Diameter	0.00005 m
Maximum Diameter	0.00236 m

Table 2 Numerical scheme and solution methods.

Variable	Setting
Turbulence model	Realizable-k-ε
Pressure velocity coupling	Phase coupled SIMPLE
Gradient	Green-Gauss node based
Momentum	Second order
Volume fraction	QUICK
Turbulence Kinetic Energy	Second order
Turbulence Dissipation rate	Second order
Transient Formulation	Second order implicit
Initialization	Hybrid initialization
Time step	0.01sec
Maximum iteration per time step	20

5. Result and Discussion

The velocity is considered as crucial parameter in the flow as well as erosion behavior at downstream of the control structure as the erosion is directly proportional to magnitude of velocity. Figure 3.1 shows the velocity contour of flow domain at trapezoidal weir and trapezoidal weir with sloping apron. Form the figure it is observed that the velocity at downstream of trapezoidal weir is quite higher than the trapezoidal weir with sloping apron. Maximum velocity at trapezoidal weir is 0.835 ms^{-1} and trapezoidal weir with sloping apron is 0.505 ms^{-1}. in case A and B, just upstream at bottom of the structure the velocity is very less due to the sudden obstruction which indicate in blue color. In case A at bed of downstream side the high velocity magnitude (yellow color) surrounded by low velocity magnitude (blue color) indicates the flow separation. But in case B just above the apron high velocity magnitude surrounded by low magnitude of velocity which leads the flow separation.

Figure 3.2 shows the longitudinal velocity distribution of flow domain for both cases. In case A, observed negative velocity found at downstream side of the structure which looks in blue color indicates that development of vortex flow and flows towards opposite direction of mean flows. In case B also found the same vortex flow at above the apron. Distribution of vertical velocity for case A and case B are shown in the figure 3.3. The maximum velocity is observed at crest of the control structure in both the cases but magnitude is high in case B than case A. In case B vertical velocity is less at downstream side when compared to upstream side of the structure but in case A at 7m from inlet there is small changes in the magnitude other than that minor variation in vertical velocity throughout the domain.

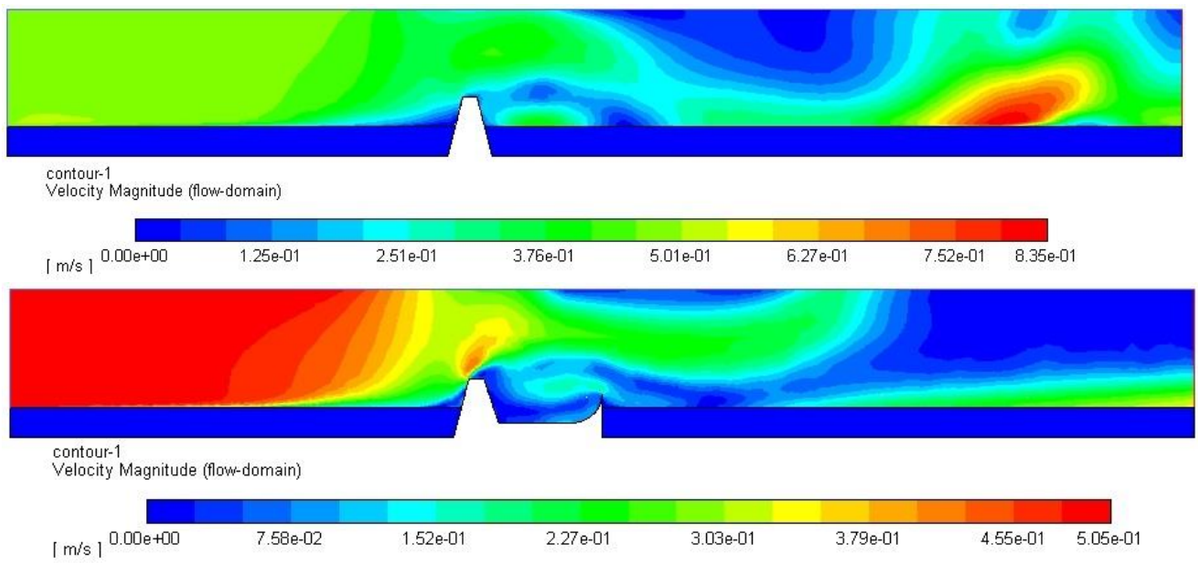

Figure 3.1 Contour of mean velocity of flow domain at trapezoidal weir and weir with sloping apron.

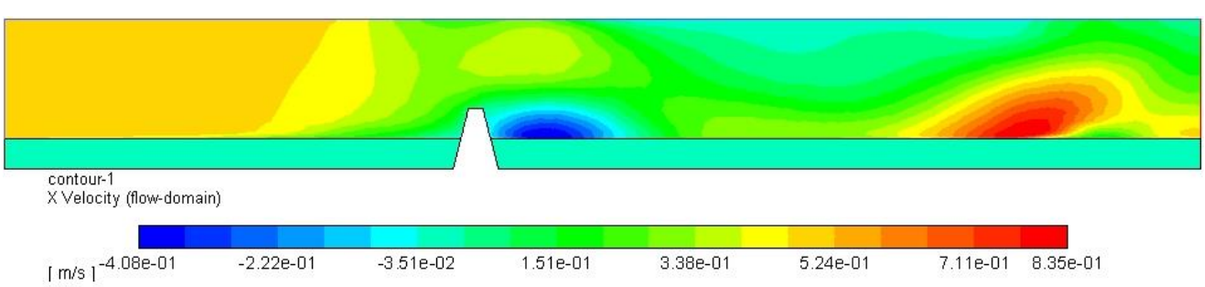

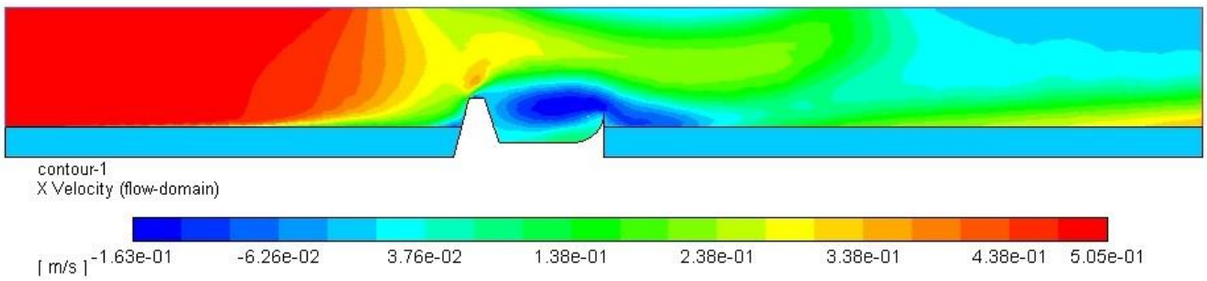

Figure 3.2 Contour of Longitudinal velocity of flow domain at trapezoidal weir and weir with sloping apron.

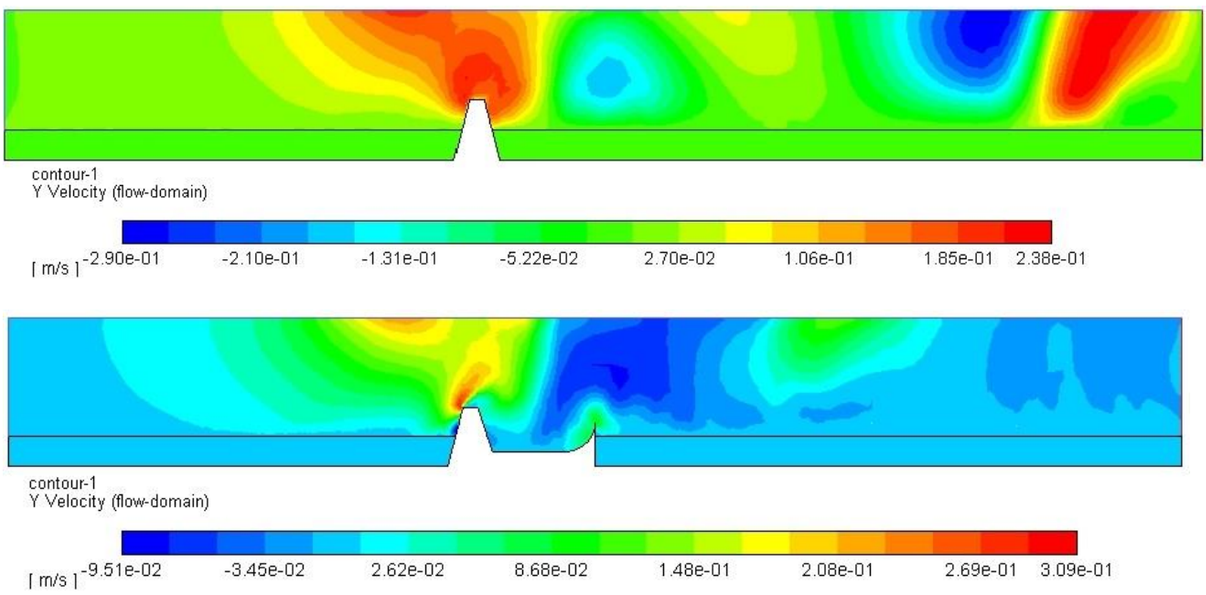

Figure 3.3 Contour of vertical velocity of flow domain at trapezoidal weir and weir with sloping.

Figure.3.4. depicts that the velocity vectors of flow domain at trapezoidal weir and weir with sloping apron. In both the cases, vector magnitude and color indicates that velocity is high at upstream and above the structure but once the flow crossed the structure the velocity is reduced drastically. A secondary Swirl flow zone is developed at bottom of the jet flow which leads to the flow separation can be visualized through vector plot at downstream side of structure in case A and above the apron in case B, the similar flow features were experienced by previous researchers Faruquzzaman Bhuiyan, A. B. M., & Hey, R. (2007).

Stream lines provide better understanding to visualize how the flow passes over the control structures. Figure.3.5 (a) and 3.5 (b) shows the stream lines or path lines of flow domain for both cases. There is a small eddy flow generated on the upstream side of the control structure due to back flow of the obstruction which can be visualized through fig. 3.5(b). In both cases a strong Secondary Circular Flow Zone (SCFZ) is generated at downstream side of the weir. The magnitude of secondary circular flow zone playing a vital role to the development of scour hole, as per the observation of Dawei Guan et al. (2014). Due to the SCFZ, the flow separation occurred at downstream side of the weir but at downstream end of the SCFZ the flow started to re-attach with the main flow which called point of re-attachment (Hoffmans, G. J., and Pilarczyk, K. W. 1995) which is clearly showing at figure 3.5.b in a closer manner. In case B two secondary circular flow zones are formed above the apron. One of them is closer to the surface of the apron and magnitude is weak in nature, while the other is above the weak secondary circular flow zone and magnitude is strong in nature. This kind of formation of two secondary circular flow zones is unique and is not observed in case A which needs to be explored further. Majority of the erosion causing secondary vortices are lies above the apron structure in case B but in case A the erosion causing SCFZ are

formed at bed surfaces of downstream side with high magnitude. Again in case B one more SCFZ are formed at sill end of the sloping bucket of apron which may lead erosion at downstream of weir but magnitude of SCFZ is very less when compared to case A. In both case A and case B the flow starts to regain its original properties and become strong after the point of reattachment. It is found that in case A one more circular flow zone is again formed at around 7m from the inlet which is very strong near the bed.

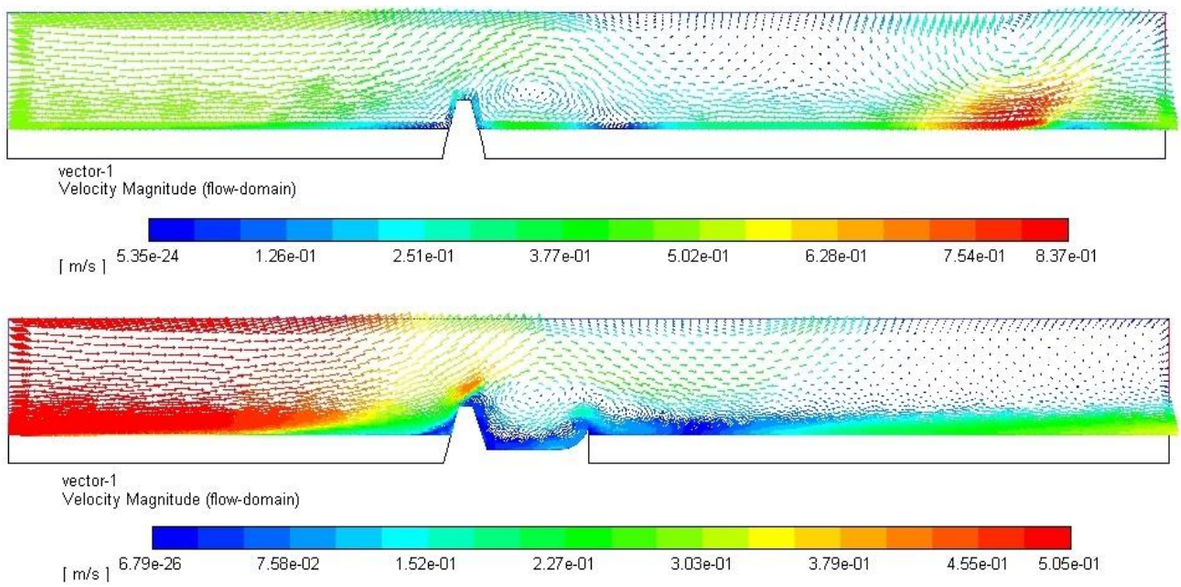

Figure 3.4 velocity vector of flow domain at trapezoidal weir and weir with sloping apron at end.

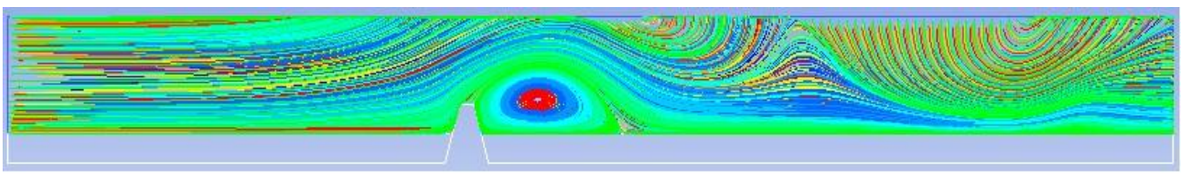

Figure 3.5 (a) Stream lines of flow domain at trapezoidal.

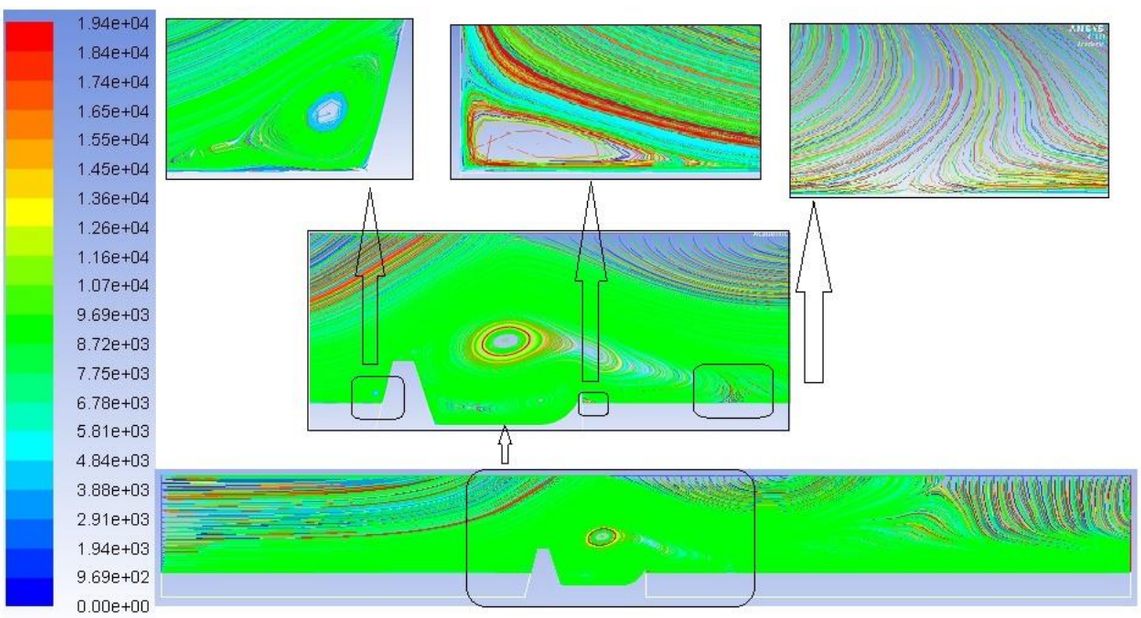

Figure 3.5 (b) stream lines of flow domain at trapezoidal weir cum sloping apron at end.

The total pressure variation of flow domain for both case A and B is illustrated in figure 3.6. The maximum pressure for Case A is 3.21 e+02 Pa and that of case B is 1.31 e+02 Pa. Pressure at the upstream side of the control structure is higher than the downstream side of the control structure. In both

case A and B, the pressure value plunges to negative at the secondary circular flow zone formed near the downstream side of the control structure. In case A, pressure value at downstream side is -9.02 e+01 Pa and in case B it is -3.83 e+01 Pa. On comparing both the cases it is observed that maximum pressure in case A is higher than case B.

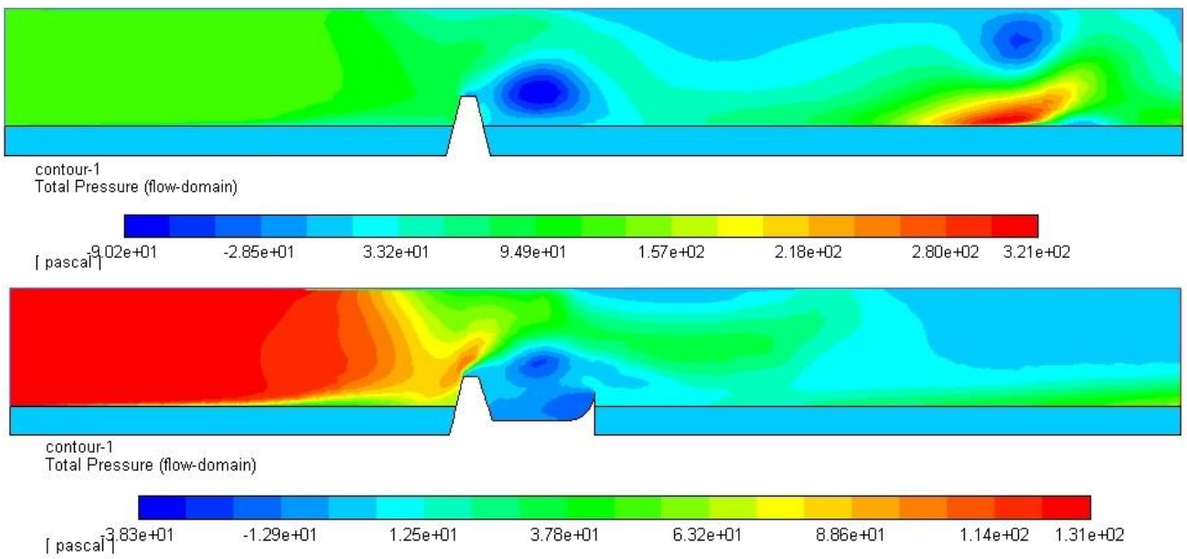

Figure 3.6 Contour of Total pressure of flow domain at trapezoidal weir and weir with sloping apron.

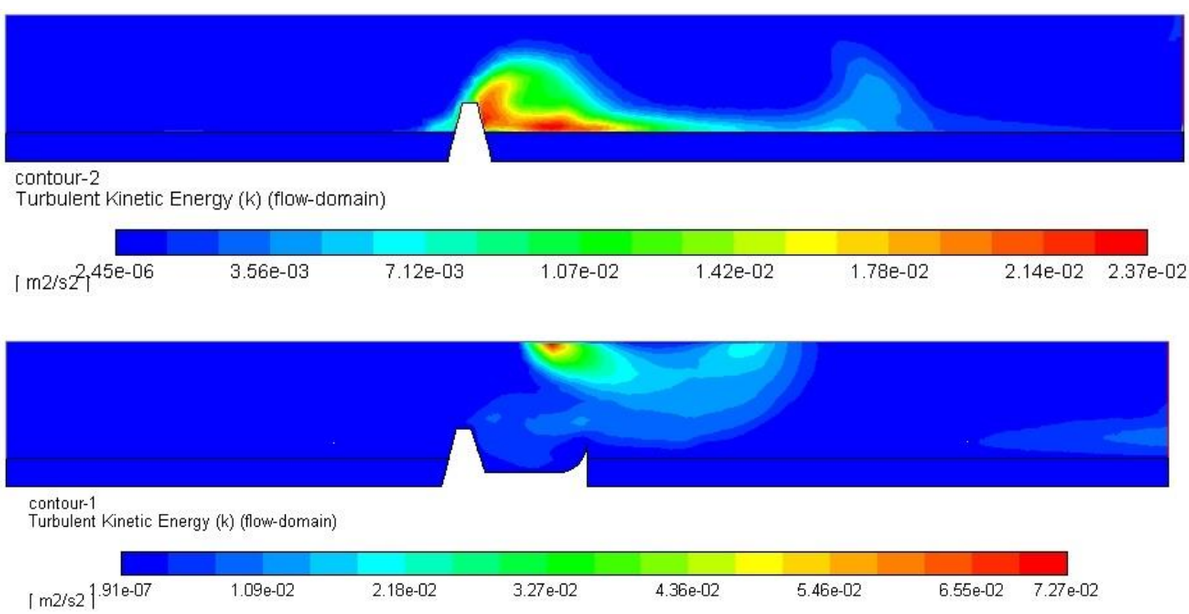

Figure 3.7 Contour of Turbulent kinetic energy of flow domain at trapezoidal weir and trapezoidal weir with sloping apron.

Generally above the crest and at the downstream of the control structure the flow is highly turbulent in nature. Figure 3.7 shows the characteristics of turbulent kinetic energy of flow domain with trapezoidal weir and trapezoidal weir with sloping apron. In case A, the maximum value of turbulent kinetic energy is 2.31 e-02 Occurring near the bed on downstream of control structure and in case B, it is 6.55 e-02 located above the sloping apron near the free surface of the flow. Turbulent viscosity, turbulent viscosity ratio and Reynolds number of flow domain also follows similar trend as of turbulent kinetic energy for each case.

Particle velocity at 50 sec is depicted in figure 3.8 and 3.9 for case A and case B respectively. The minimum particle velocity in case A is 1.26 e-03 ms^{-1} with majority of the particles velocity lying in the range of 3.59 e-01 to 3.99 e-01 ms^{-1} with very few particles gaining more velocity than this. In a similar

fashion the minimum velocity for case B is 2.78 e-05 ms^{-1} with majority of the particles velocity lying in the range of 3.2e-01 to 3.55e-01 ms^{-1}. The velocity of particle impingement is another important parameter which causes erosion. In case A the particles are directly hitting the bed surface and their velocity is very high at the bed surface which leads to scour formation at downstream of structure. While in case B most of the particles are in suspension and particle velocity at bed surface is very less compared to case A.

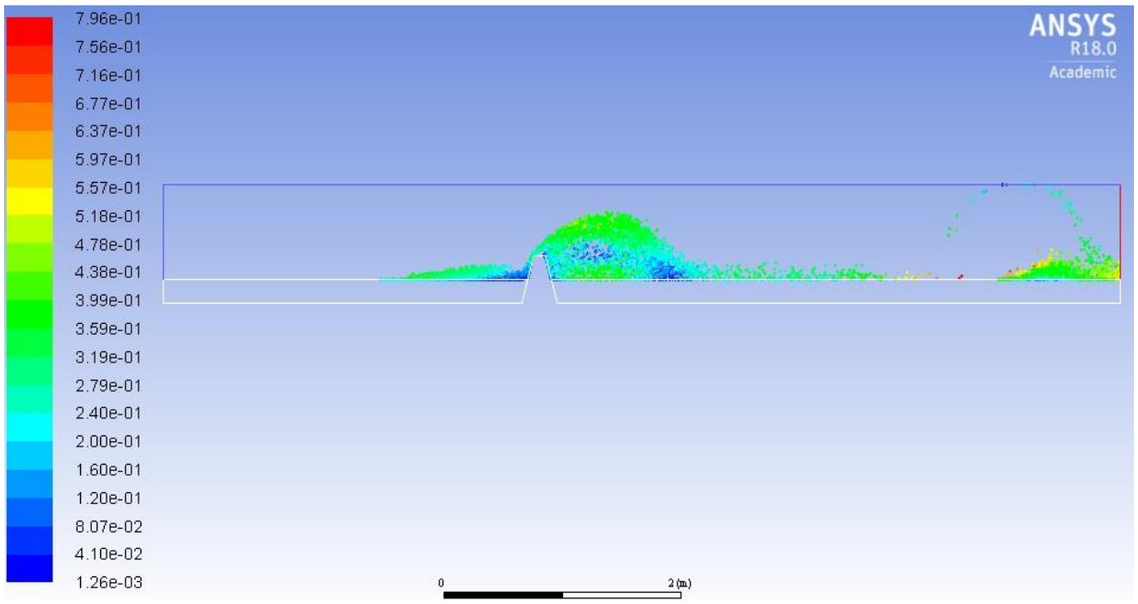

Figure 3.8 Contour of particle velocity of flow domain at trapezoidal weir.

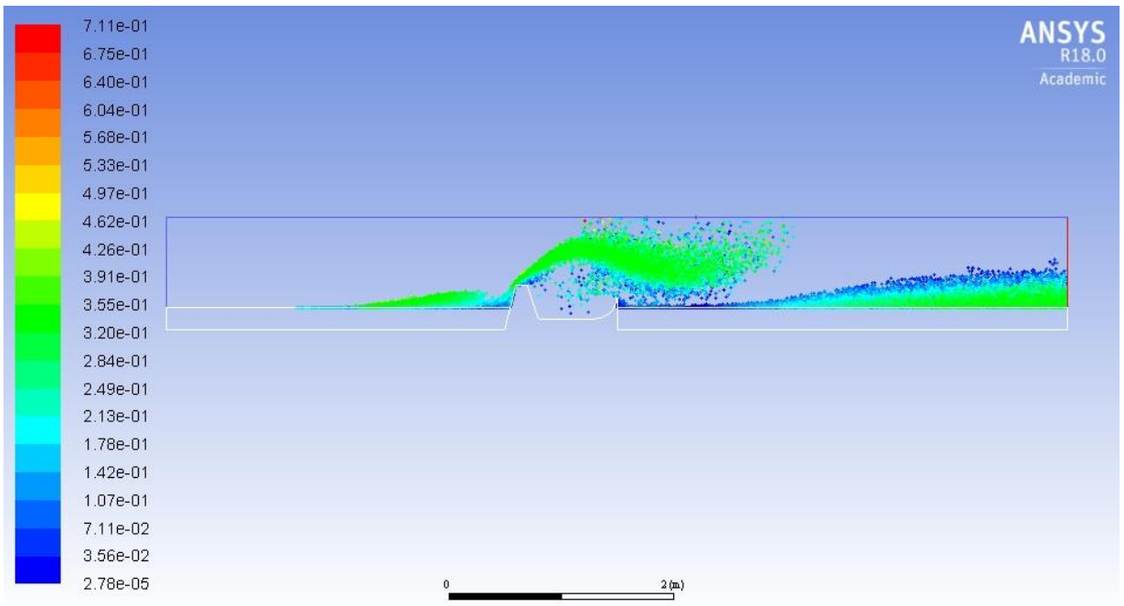

Figure 3.9 Contour of particle velocity of flow domain at trapezoidal weir with sloping apron.

Figure 4.0(a) shows the velocity of flow domain of trapezoidal weir and figure 4.0(b) shows the trapezoidal weir with sloping apron. In both cases the initial inflow velocity is 0.5 ms^{-1}. In upstream region of case A the flow velocity reduces from 0.5 ms^{-1} at the inlet to 0.39 ms^{-1} near the control structure. The flow velocity increases just above the crest of the structure and reduces once it crosses the structure with maximum velocity of 0.85 ms^{-1} observed at 7 m from inlet. In upstream region of case B, the flow velocity reduces from 0.5 ms^{-1} at inlet to 0.325 ms^{-1} near the control structure. Just above the crest of the structure, velocity increases with a narrow peak region and further decreases at the downstream of structure. The maximum velocity in case B is the inlet velocity and spans up to 2 m from inlet. In case A,

the maximum velocity is higher than inlet velocity and in case B maximum velocity is almost equal to inlet velocity. The final comparison of both cases shows that the use of trapezoidal weir with sloping apron in case B reduces the flow velocity in the downstream region which ultimately reduces the scour formation.

Shear stress distribution at the sand bed is shown in figure 4.1 for both cases. In both cases a small peak in shear stress is observed at around 2.5 m from the inlet due to secondary circular flow formation. In case B it is clearly visible and in case A it is not clearly visible due to the band of scale. In case A the maximum shear stress reaches nearly 1.01 e+00 and in case B it is around 1.30 e-01.

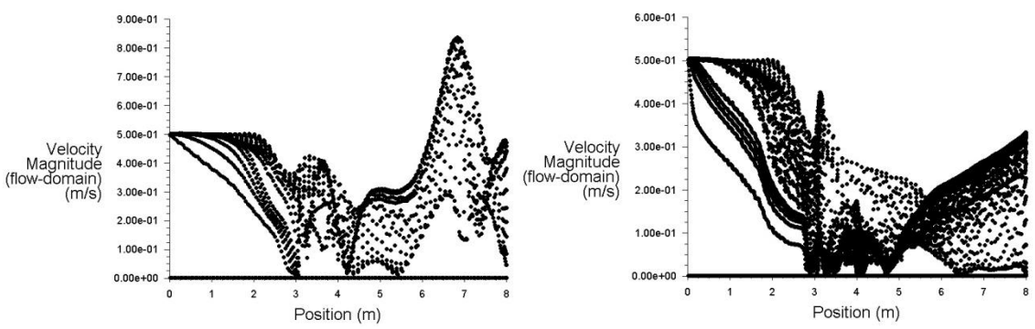

Figure 4.0 Velocity magnitudes at trapezoidal weir (left) and at trapezoidal weir with sloping apron (right).

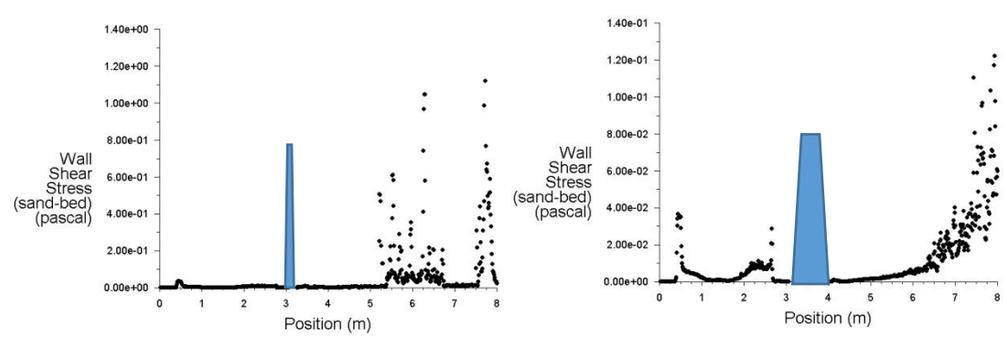

Figure 4.1 Shear stress at trapezoidal weir (left) and at trapezoidal weir with sloping apron (right).

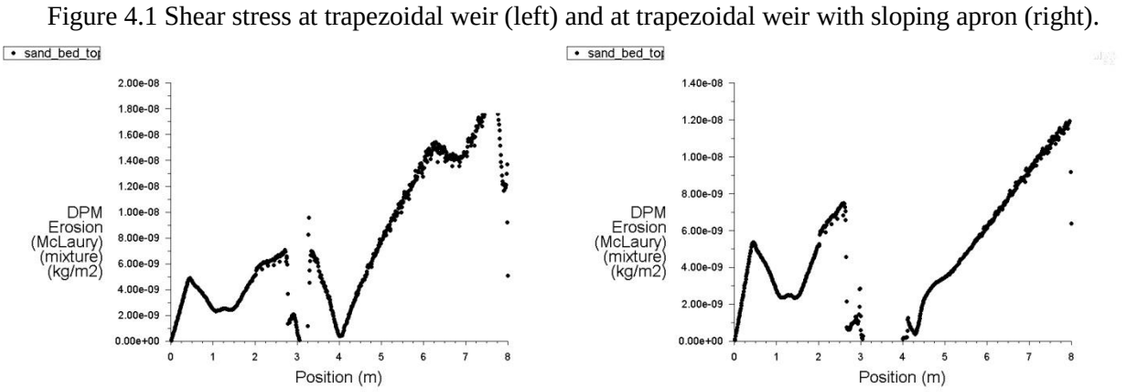

Figure 4.2 Erosion rate at trapezoidal weir (left) and at trapezoidal weir with sloping apron (right).

Figure 4.2 shows the erosion rate for 50 sec of Mc. Laury model for trapezoidal weir and trapezoidal weir with sloping apron. The erosion starts from inlet and at 0.5 m there is a small change in the erosion rate and one more peak is also observed at upstream side of the control structure. The erosion rate and its behavior is quite similar in the upstream side of the structure for both cases. In case A the downstream erosion rate is nearly 1.00 e-08 kg m^{-2} which is higher than upstream side erosion rate. At 4.3 m from inlet the erosion rate is very less which indicates that there is a deposition at end of the secondary circular flow zone. Beyond 4.3 m the erosion rate is increasing and it reaches the maximum

value at outlet which is equal to 1.80 e-08 kg m^{-2}. In case B very less erosion rate is observed close to the structure in the downstream region as compared to the upstream region and followed by deposition at end of the small secondary circular flow zone. Again the erosion rate is increasing further until it reaches the outlet where the maximum erosion rate is 1.20 e-08 kg m^{-2} which is less than case A.

6. Conclusion

This study mainly intended to study the flow features and its associated scour at the downstream of control structure and to reduce the scour at downstream side which could leads towards the failure of the entire structure. From the present study it was able to visualize the secondary circular flow zone at both upstream and downstream sides of control structure. In case B above the apron, two secondary circular flow zone is generated this is unique and needs to be explored further. DDPM model gives the provision of visualizing the particle tracking with different parameters like particle residence time, particle velocity in longitudinal and vertical direction, particle swirl velocity, particle diameter, particle Reynolds number and many other properties. In case B downstream velocity is very less than in case A and it is observed that the magnitude of scour at the downstream of trapezoidal weir is higher than scour formed near the trapezoidal weir with sloping apron. The high level of turbulence formed near the surface in case B aids in capturing more dissolved oxygen into the water from the atmosphere which is helpful for aquatic life. Hence this type of weir with sloping apron proved to be a better engineering solution towards better life expectancy.

Notation:

$\vec{v}_p$ = Velocity of phase p

$\dot{m}_{qp}$ = Characterizes the mass transfer from the “q” phase to “p” phase

$\dot{m}_{qp}$ = Characterizes the mass transfer from the “p” phase to “q” phase.

α_p = Volume fraction.

ρ_p = Density of the phase p.

G_k = Generation of turbulence kinetic energy due to mean velocity gradients.

G_b = Generation of turbulence kinetic energy due to buoyancy.

C_2, $C_{3\varepsilon}$ and $C_{1\varepsilon}$ are constants.

σ_k = Turbulent Prandtl numbers for K.

σ_ε = Turbulent Prandtl numbers for ε.

Y_m = Contribution of the fluctuating dilation in compressible turbulence to the overall dissipation rate.

μ_p = Shear viscosity of phase p.

$F_{vm,lift,user}$ = Virtual mass force, lift force and user specified force.

$S_{DPM,explicit}$ = Momentum exchange term for explicit.

$\vec{v}_{DPM}$ = Momentum exchange term for implicit.

K_{DPM} = Particle averaged interphase momentum exchange coefficient.

F = Empirical constant,

V = Particle impact velocity,

Bh = Brinell’s hardness number of wall material,

K = Constant for material property

γ = Particle impingement angle

b, c are the constant.

S_k and S_ε are User-defined source term.

References

Akoz, M. S., Gumus, V., & Kirkgoz, M. S. (2014). Numerical simulation of flow over a semicylinder weir. *Journal of Irrigation and Drainage Engineering*, *140*(6), 04014016. https://doi.org/10.1061/(ASCE)IR.1943-4774.0000717

Ansys Fluent 18.0 User Manual (2017), Ansys Inc.,

Bormann, N. E., and Julien, P. Y. (1991). Scour downstream of grade-control structures. *Journal of Hydraulic Engineering*, *117*(5), 579-594. https://doi.org/10.1061/(ASCE)0733-9429(1991)117:5(579)

D'Agostino, V., & Ferro, V. (2004). Scour on alluvial bed downstream of grade-control structures. *Journal of Hydraulic Engineering*, *130*(1), 24-37. https://doi.org/10.1061/(ASCE)0733-9429(2004)130:1(24)

Dey, S., & Sarkar, A. (2006). Scour downstream of an apron due to submerged horizontal jets. *Journal of hydraulic engineering*, *132*(3), 246-257. https://doi.org/10.1061/(ASCE)0733-9429(2006)132:3(246)

Faruquzzaman Bhuiyan, A. B. M., and Hey, R. (2007). Computation of three-dimensional flow field created by weir-type structures. *Engineering Applications of Computational Fluid Mechanics*, *1*(4), 350-360. https://doi.org/10.1080/19942060.2007.11015205

Guan, D., Melville, B., & Friedrich, H. (2016). Local scour at submerged weirs in sand-bed channels. *Journal of Hydraulic Research*, *54*(2), 172-184. https://doi.org/10.1080/00221686.2015.1132275

Guan, D., Melville, B. W., & Friedrich, H. (2013). Flow patterns and turbulence structures in a scour hole downstream of a submerged weir. *Journal of Hydraulic Engineering*, *140*(1), 68-76. https://doi.org/10.1061/(ASCE)HY.1943-7900.0000803

Hoffmans, G. J., & Booij, R. (1993). Two-dimensional mathematical modelling of local-scour holes. *Journal of Hydraulic Research*, *31*(5), 615-634. https://doi.org/10.1080/00221689309498775

Hoffmans, G. J., & Pilarczyk, K. W. (1995). Local scour downstream of hydraulic structures. *Journal of Hydraulic Engineering*, *121*(4), 326-340. https://doi.org/10.1061/(ASCE)0733-9429(1995)121:4(326)

Kang, S., & Sotiropoulos, F. (2015). Numerical study of flow dynamics around a stream restoration structure in a meandering channel. *Journal of Hydraulic Research*, *53*(2), 178-185. https://doi.org/10.1080/00221686.2015.1023855

Lv, X., Zou, Q., & Reeve, D. (2011). Numerical simulation of overflow at vertical weirs using a hybrid level set/VOF method. *Advances in water resources*, *34*(10), 1320-1334. https://doi.org/10.1016/j.advwatres.2011.06.009

Michael Scurlock, S., Thornton, C. I., & Abt, S. R. (2015). One-Dimensional Modeling Techniques for Three-Dimensional Grade Control Structures. *Journal of Hydraulic Engineering*, *141*(5), 05015001. https://doi.org/10.1061/(ASCE)HY.1943-7900.0000950

Muller, S., Guiraud, P., & Line, A. (2011). Particle bed deformation in front of a weir induced by subcritical laminar flow. *Journal of Hydraulic Research*, *49*(2), 194-204. https://doi.org/10.1080/00221686.2011.552460

Nguyen, V. T., & Nestmann, F. (2004). Applications of CFD in hydraulics and river engineering. *International Journal of Computational Fluid Dynamics*, *18*(2), 165-174. https://doi.org/10.1080/10618560310001634186

Nguyen, V. T., Moreno, C. S., & Lyu, S. (2015). Numerical simulation of sediment transport and bedmorphology around Gangjeong Weir on Nakdong River. *KSCE Journal of Civil Engineering*, *19*(7), 2291. https://doi.org/10.1007/s12205-014-1255-y

Noor, M. M., Wandel, A. P., & Yusaf, T. (2013, July). Detail guide for CFD on the simulation of biogas combustion in bluff-body mild burner. *In Proceedings of the 2nd International Conference of Mechanical Engineering Research (ICMER 2013)* (pp. 1-25). Universiti Malaysia Pahang.

Oertel, M., BALMES, J., & BUNG, D. B. Numerical simulation of erosion processes on crossbar block ramps.

Pagliara, S., Palermo, M., Kurdistani, S. M., & Sagvand Hassanabadi, L. (2015). Erosive and hydrodynamic processes downstream of low-head control structures. *Journal of Applied Water Engineering and Research*, *3*(2), 122-131. https://doi.org/10.1080/23249676.2014.1001880

Parsi, M., Najmi, K., Najafifard, F., Hassani, S., McLaury, B. S., & Shirazi, S. A. (2014). A comprehensive review of solid particle erosion modeling for oil and gas wells and pipelines applications. *Journal of Natural Gas Science and Engineering*, *21*, 850-873. https://doi.org/10.1016/j.jngse.2014.10.001

Qu, J., Ramamurthy, A. S., Tadayon, R., & Chen, Z. (2009). Numerical simulation of sharp-crested weir flows. *Canadian Journal of Civil Engineering*, *36*(9), 1530-1534. https://doi.org/10.1139/L09-067

Rajaratnam, N., & Nwachukwu, B. A. (1983). Flow near groin-like structures. *Journal of Hydraulic Engineering*, *109*(3), 463-480. https://doi.org/10.1061/(ASCE)0733-9429(1983)109:3(463)

Sinha, S. K., & Marelius, F. (2000). Analysis of flow past submerged vanes. *Journal of Hydraulic Research*, *38*(1), 65-71. https://doi.org/10.1080/00221680009498360

Tingsanchali, T., & Maheswaran, S. (1990). 2-D depth-averaged flow computation near groyne. *Journal of Hydraulic Engineering*, *116*(1), 71-86. https://doi.org/10.1061/(ASCE)0733-9429(1990)116:1(71)

Weidner, K., Petrie, J., Diplas, P., Nam, S., Gutierrez, M., & Ellenberg, M. (2012). Numerical simulation of jet test and associated soil erosion. *ICSE6 Paris*, *609616*.